Multiwavelength digital holography with autocalibration of phase shifts and artificial wavelengths

Daniel Carl,* Markus Fratz, Marcel Pfeifer, Dominik M. Giel, Heinrich Höfler

Fraunhofer Institute for Physical Measurement Techniques IPM
Heidenhofstrasse 8, D-79110 Freiburg, Germany

**Corresponding author: daniel.carl@ipm.fraunhofer.de*

A novel implementation of lensless multiwavelength digital holography with autocalibration of temporal phase shifts and artificial wavelength is presented. The algorithm we used to calculate the phase shifts was previously proposed [Opt. Lett. **29,** 183 (2004)] and, to our knowledge, is now used for the first time in lensless holography. Because precise knowledge of the generated artificial wavelength is crucial for the absolute measurement accuracy, a simple and efficient method to determine the artificial wavelength directly is presented. The calibration method is based on a simple modification of the experimental setup and needs just one additional image acquisition per wavelength. The results of shape measurement of a metallic test object with rough surface and steep edges are shown and the measurement accuracy is discussed.

OCIS codes: (090.0090) Holography, (090.1995) Digital holography, (090.4220) Multiplex holography, (120.6165) Speckle interferometry, metrology, (120.5050) Phase measurement.

1. Introduction

Digital holography and interferometry are well-established tools for nondestructive testing in industrial applications [1-7]. In digital holography the lateral resolution of the reconstructed holographic image is limited by the pixel pitch of the image-recording device, typically a CCD or complementary metal oxide semiconductor (CMOS) sensor, and can be improved with a lens. In combination with microscopy, digital holography enables quantitative phase measurement of microscale technical objects and biological samples. Thus it has become a versatile tool also for marker-free living cell analysis [8-14]. Several approaches to overcome the ambiguity between refractive index and thickness measurement of transparent objects, such as living cells, in transmission light arrangements have been published [15-17].

Application of digital holography to sophisticated industrial measurement tasks is often restricted by phase ambiguities that are due to the limited wavelength and the resulting restriction of the dynamic range. Spatial unwrapping can overcome this problem but often fails, e.g. at steep edges and deep holes [18]. Furthermore, optically rough surfaces that are common in industrial processing generate a speckle pattern with quasi-random phase distribution under coherent illumination. Therefore, reconstructed phase maps yield no directly accessible information of the geometrical shape of an object. To overcome both restrictions, the recording of digital holograms at multiple wavelengths is a well-established approach [19-26]. Both temporal [21] and spatial [24,25] phase-shifting techniques have been applied to multiple-wavelength holography.

The correlation between two speckle fields captured at identical boundary conditions but at different wavelengths allows numerical generation of phase maps of an artificial wavelength by subtracting reconstructed phase maps at different wavelengths from each other modulo 2π. In recent years, affordable tunable diode lasers with external resonators have been developed [27]. Tuning is performed by tilting a Bragg grating. Temperature changes of the setup can be suppressed or controlled carefully in a laboratory but not as easily in an industrial environment; thus, spectral long-term drifts cannot be excluded. The error in the difference between the two wavelengths is inversely proportional to the absolute accuracy of

the phase measurement. Different approaches to determine the maximum allowable measurement error have been presented [22, 25] from which it can be seen that highly precise wavemeters must be used to monitor and control the respective single wavelength, which is an expensive solution of the problem. Here we present a simple and useful method to monitor the generated artificial wavelength directly.
To avoid reconstruction of disturbing terms such as twin image and zero-order images, spatial phase-shifting techniques can be combined with complex wave field propagation [8,9]. In digital holographic microscopy with a spatial phase shift the setup can be arranged in such a way that the lateral resolution is diffraction limited if the image magnification and thus the microscope objective are chosen appropriately with respect to the pixel pitch of the applied sensor [8,12,16]. However, spatial phase-shifting techniques are always connected with a loss in space-bandwidth product. To avoid this loss in our lensless setup, we combined temporal instead of spatial phase shifting with complex wave field propagation. For this purpose the temporal phase steps usually have to be controlled carefully, e.g., with a closed-loop controlled piezoelectric actuator. To keep the setup simple and affordable, we present the application of an efficient algorithm to calculate phase differences between subsequently recorded interferograms that, to our knowledge, are used for the first time in lensless digital holography [26].

2. Experimental Procedure

A. Setup

Figure 1 shows an experimental setup for lensless digital holography. A tunable diode laser with an external cavity (DL100, TOPTICA Photonics, Munich, Germany) is used as illumination device [27].

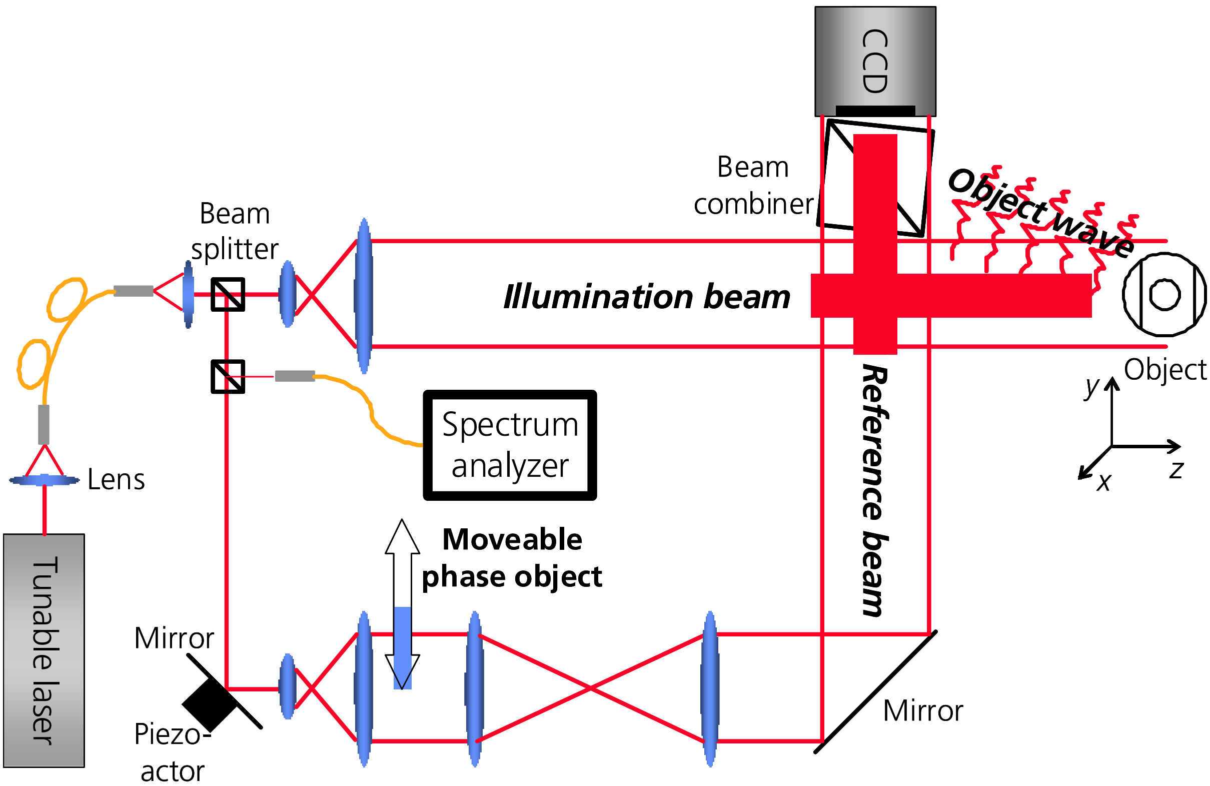

Fig 1: Experimental setup for temporal phase-shifting lensless multiwavelength digital holography with moveable reference object (BK7 glass plate, *d*=3.0 mm).

The wavelength of the diode laser is tuned by tilting an external grating with a stepper motor. The typical linewidth of the diode laser is specified to be between 0.5 and 1 MHz. The minimum artificial wavelength is restricted by a tuning range of approximately 8 nm, whereas the maximum is restricted by the spectral stability of the system and the repeatability of the tuning unit (tilt of the external grating, diode current, and temperature control).

Using this laser source, repeatable generation of artificial wavelengths from approximately 75 µm up to several centimeters is possible. To avoid beam misalignment that is due to tuning, the beam is coupled into a single-mode fiber. To guarantee mode-hop-free operation during the measurement and to monitor the actually emitted wavelength, a spectrum analyzer is applied. After having passed through the glass fiber, the light is collimated and divided into an object wave and a reference wave. Both are expanded to fit the size of the object and the camera chip, respectively. The reference wave is deflected by a mirror mounted on a piezostage to achieve temporal phase shifts between the object wave and the reference wave. The piezostage runs in open-loop mode.

Additionally, a movable phase object is located in the reference path to measure the generated artificial wavelength directly as described below. It is illuminated by the expanded reference beam and imaged onto the CCD sensor. Finally, the reference wave and the diffracted object wave – usually a speckle pattern – are superimposed by a beam combiner. The spatial intensity distribution of the generated digital hologram is captured by an 8 bit CCD camera with 1392 x 1040 pixels, 4.65 µm pixel pitch, and IEEE1394 interface (Marlin, Allied Vision Technologies, Stadtroda, Germany). In the depicted setup a small angle between illumination and observation is realized by tilting the beam combiner slightly to suppress disturbing interferences that are due to reflections. In this case the interferometer sensitivity vector must be taken into account for conversion of the quantitative phase measurement to a geometric shape measurement [28].

B. Hologram Acquisition

To perform shape measurements with the described setup, holograms with different appropriate wavelengths λ_1, λ_2, a minimum two, are recorded. For each wavelength λ_i (i=1, 2 ...) a minimum of three phase-shifted speckle interferograms of the same object state must be captured. Figure 2(a) shows three speckle interferograms of our test object. The phase shifts between interferograms φ_1 and φ_2 are performed by an uncontrolled piezoelectric actuator and thus the induced phase shifts are in the range from 90° to 150° and not known *a priory*. Additionally, one additional interferogram with a phase object shifted partly into the reference path of the interferometer is recorded for each wavelength. Here a 3 mm thick BK7 glass plate and well-known refractive index (n_{BK7}=1.51118 at 780 nm) serve as the reference object. Therefore the reference object is imaged sharply onto the hologram plane (CCD sensor plane). Its edge is clearly visible as a dark stripe in Fig. 2(b). Two regions of interest (ROIs) are defined: ROI1 on the side without a phase object and ROI2 on the side with a phase object. It is shown that there is no additional phase shift between the third interferogram with the piezoelectric actuator in Figs. 2(a) and (b). As a result, the phase shift in ROI1 should be close to zero, whereas the phase shift in ROI2 is induced by the well-known phase object. Global phase shifts induced, e.g., by vibrations are assumed to be negligible.

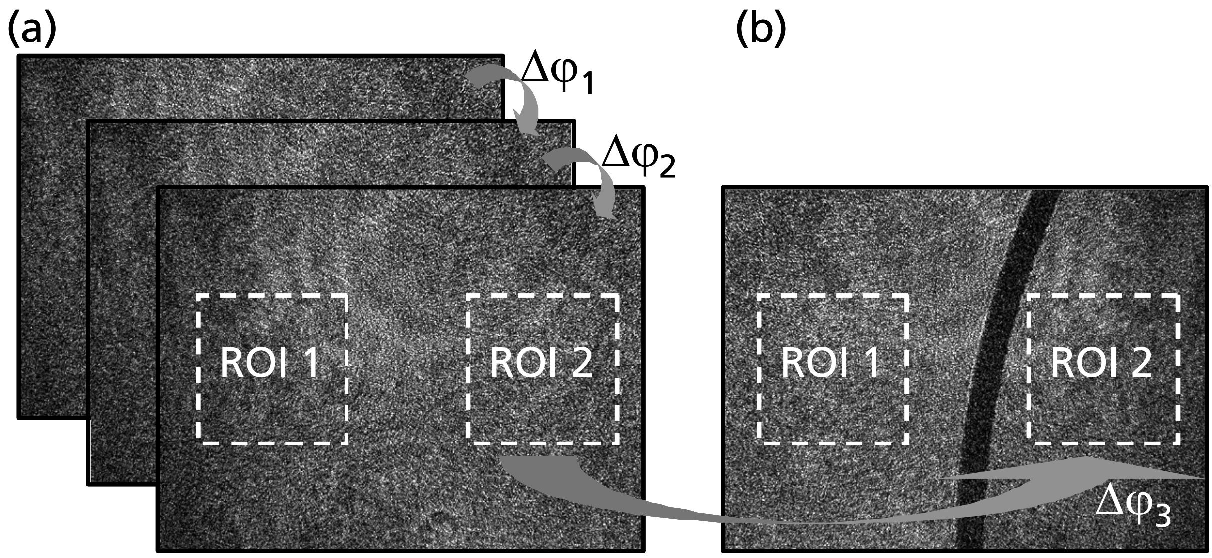

Fig. 2: (a) Three temporal phase-shifted speckle interferograms of a single object state and (b) additionally captured interferogram with the phase object (3.0 mm BK7 glass plate) moved partly into the reference path of the interferometer.

3. Numerical Reconstruction

Numerical reconstruction of the object wave is performed in three steps:

1. determination of the global phase shifts between the captured speckle interferograms;
2. calculation of the complex object wave within the hologram by temporal phase shifting;
3. propagation of the complex object wave (hologram) to the object plane.

A. Temporal Phase-Shifting with Unknown Phase Steps

In Ref. [1] Cai *et al*. described a general method for extracting unknown and unequal phase steps from sequentially recorded interferograms. The algorithm works on both smooth and diffuse objects and is usable for any number of interferograms N ($N \geq 3$). The phase steps φ_1 and φ_2 that are introduced by the piezoelectric actuator (see Fig. 1) are calculated based on the statistical nature of the diffraction field. In a first step averaged intensity differences between subsequently captured interferograms are calculated as shown in Eqs. (1) and (2) where M is the number of pixels of interferogram number i with discrete intensity distribution $I_i(x,y)$. Variables x and y represent discrete pixel numbers. In a first step the auxiliary constants p, q, r, and c are calculated as:

$$\begin{aligned} p &= \frac{1}{M}\sum_{x,y}\left|I_1(x,y) - I_2(x,y)\right| \\ q &= \frac{1}{M}\sum_{x,y}\left|I_2(x,y) - I_3(x,y)\right| \\ r &= \frac{1}{M}\sum_{x,y}\left|I_1(x,y) - I_3(x,y)\right| \\ c &= 2pqr\left[2\left(p^2q^2 + p^2r^2 + q^2r^2\right) - \left(p^4 + q^4 + r^4\right)\right]^{-1/2} \end{aligned} \tag{1}$$

In the next step, the global phase shifts φ_1 and φ_2 are calculated by insertion of constants p, q, r, and c:

$$\varphi_1 = 2\arcsin(p/c), \quad \varphi_2 = 2\arcsin(q/c) \tag{2}$$

Further improvement of φ_1 and φ_2 by an iterative approach is also described in [1] but not applied here because no significant reduction of noise was measured in our data.
Finally, insertion of φ_1 and φ_2 in Eq. (3) and assumption of a constant spatial intensity distribution of the reference wave result in the complex hologram $C_\lambda(x,y)$, where λ denotes the respective recording wavelengths of the interferograms:

$$C_\lambda(x,y) = \frac{\exp(i\varphi_1/2)}{\sin[(\varphi_1-\varphi_2)/2)]}(I_1(x,y)-I_3(x,y)) - \frac{\exp[i(\varphi_1-\varphi_2)/2)]}{\sin(\varphi_1/2)}(I_1(x,y)-I_2(x,y)) \tag{3}$$

In comparison with [1] a global real factor is neglected because of a reference wave with nearly constant intensity across the CCD plane. The factor affects only the scale of the reconstructed spatial intensity distribution in the CCD plane.

B. Propagationand Difference Phase

Reconstruction of the shape of the object under investigation is performed by numerical propagation of each complex hologram $C_\lambda(x, y)$ to the object plane, i.e., the plane in which the object is located. For this the wavefield in front of the camera is reconstructed numerically. This reconstruction is performed by numerical approximation of the Fresnel-Kirchhoff diffraction integral. If the numerical reconstruction is limited to the paraxial region, i.e., $x^2+y^2<<z^2$ with z denoting the distance between the camera and the object plane, the Fresnel-Kirchhoff diffraction integral can be approximated by a convolution of the complex hologram $C_\lambda(x,y)$ in the camera plane and the impulse response of free-space propagation [7]:

$$\Psi_{z,\lambda}(x,y) \approx \mathrm{FFT}^{-1}\left\{\mathrm{FFT}[C_\lambda(x,y)]\exp\left[-i\pi\lambda z\left(\frac{x'^2}{\Delta x^2 N_x^2}+\frac{y'^2}{\Delta y^2 N_y^2}\right)\right]\right\} \tag{4}$$

Here FFT and FFT^{-1} denote the discrete fast Fourier transform and the inverse fast Fourier transform, respectively. $\Psi_{z,\lambda}(x,y)$ denotes the reconstructed complex object wave at recording wavelength λ with a reconstruction distance z. Numerical propagation is done for each wavelength λ separately with constant reconstruction distance z. Amplitude and phase of the reconstructed wavefronts $\Psi_{z,\lambda}(x,y)$ are calculated.
It is worth noting that the surface of the observed object must not significantly exceed the depth of focus of the numerical reconstruction. An estimation of the depth of focus is given, e.g., in Ref. [7]. Propagation of the wave field is performed by numerical approximation of the Fresnel-Kirchhoff diffraction integral by a convolution. In comparison with the Fresnel propagation the convolution method has the advantages that the sampling interval stays constant while propagating and does not depend on the illumination wavelength. This is a necessary condition for multiwavelength digital holography. The constancy of the sampling interval makes it necessary to pad the hologram with zeros before performing the numerical reconstruction; otherwise the reconstructed image is disturbed by strong aliasing effects [29,30].Considering wavelength λ, the pixel pitch of the image recording device Δx and Δy, and the reconstruction distance z, expansion to N_x=4096 and N_y=4096 pixels is adequate [29,30]. For optimal performance of the FFT the pixel numbers are chosen to be powers of 2.
From Eq. (4) the phase distribution of the diffraction field in the object plane can be calculated by extracting the complex argument of $\Psi_{z,\lambda}(x,y)$ for all used wavelengths λ_i:

$$\delta_{\lambda,i}(x,y) = \arctan\left(\frac{\mathrm{Im}\{\Psi_{z,\lambda,i}(x,y)\}}{\mathrm{Re}\{\Psi_{z,\lambda,i}(x,y)\}}\right), \tag{5}$$

where Im{} and Re{} denote the imaginary and real parts of a complex number, respectively. Difference phase maps are calculated by subtracting the reconstructed phase maps of different wavelengths modulo 2π from each other:

$$\delta_d(x,y) = \mathrm{mod}\left(\delta_{\lambda,i}(x,y) - \delta_{\lambda,j}(x,y),\ 2\pi\right). \tag{6}$$

As it is shown, e.g., in Ref. [25], the resulting difference phase map corresponds to an interferogram that would be observable if illumination were performed with a wavelength equal to the artificial wavelength given by [22, 25]

$$\lambda_a = \frac{\lambda_1\lambda_2}{|\lambda_1 - \lambda_2|} = \frac{\lambda_1\lambda_2}{\Delta\lambda} \tag{7}$$

From the difference phase map and knowledge of the artificial wavelength, a height map of the object can be calculated:

$$h(x,y) = \frac{\lambda_a}{2}\frac{\delta_d(x,y)}{2\pi}. \tag{8}$$

Multiple artificial wavelengths can be used to avoid unwrapping errors [22,26]. To accelerate calculation the described numerical reconstruction including phase shifting and propagation is performed on a Graphical Processor Unit (N295GTX-1792MB) as proposed in [31].

C. Auto Calibration

Equation (7) shows that the error of artificial wavelength λ_a is proportional to the respective single wavelengths λ_1 and λ_2 but inversely proportional to the difference $\Delta\lambda$. For large artificial wavelength the difference between the two single wavelengths $\Delta\lambda$ becomes very small, e.g., for an artificial wavelength of 10 mm generated by a tunable laser diode with a central wavelength of approximately 780 nm a difference between the two single wavelengths of 60 pm must be adjusted. Therefore, an error of 5 pm of the wavelength difference results in an 8 % error in the artificial wavelength.

We present two different methods for calibration of the artificial wavelength. The first method uses the Cai *et al.* three- or four-step algorithm [1]. For this method, three holograms without a phase object [Fig. 2(a)] and only one additional hologram with the reference object partly shifted into the interferometer's reference path [Fig. 2(b)] are recorded. Two ROIs are defined in the recorded image: one that is not influenced by the reference object (ROI1) and one in the region in which the reference object is imaged (ROI2). To apply the Cai *et al.* method for calibration of the artificial wavelength, the two regions are assumed to be independent sets of holograms.

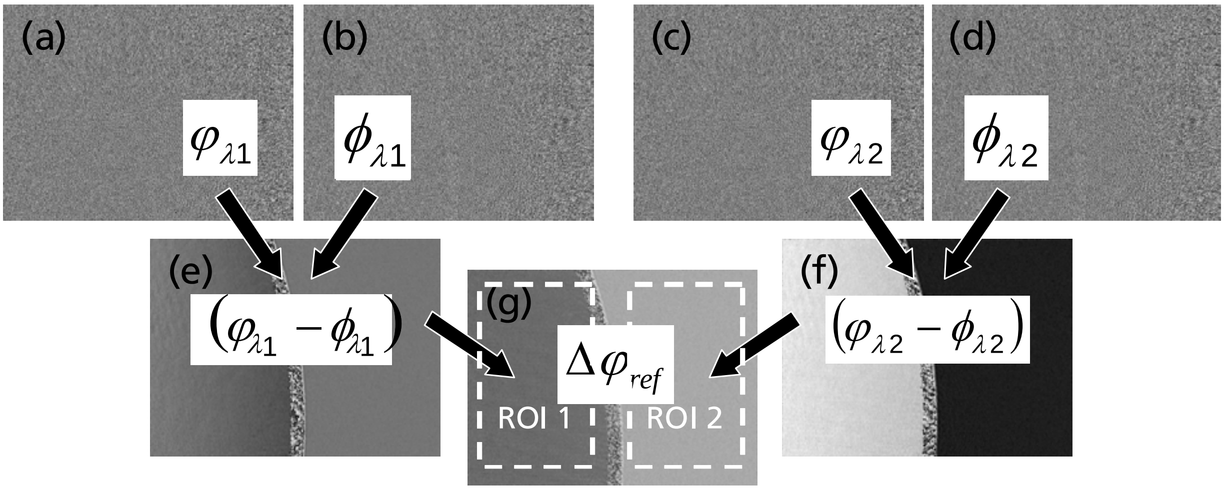

Fig. 3: (a) Reconstructed phase map $\varphi_{\lambda 1}(x,y)$ in the hologram plane without a reference object; (b) reconstructed phase map $\phi_{\lambda 1}(x,y)$ with a reference object of the same wavelength λ_1; (c), (d) corresponding phase maps $\varphi_{\lambda 2}(x,y)$ and $\phi_{\lambda 2}(x,y)$ of the second wavelength λ_2; (e) difference phase map of wavelength λ_1; (f) difference phase map of wavelength λ_2; (g) difference phase map of generated artificial wavelength λ_a, ROI1 without and ROI2 with a reference object, respectively.

Now, for both regions, global phase shifts $\Delta\varphi_{1,ROI1}$, $\Delta\varphi_{2,ROI1}$ and $\Delta\varphi_{1,ROI2}$, $\Delta\varphi_{2,ROI2}$ can be calculated using Eqs. (1) and (2). The first phase steps $\Delta\varphi_{1,ROI1}$ and $\Delta\varphi_{1,ROI2}$ are, of course, equal to each other because they were introduced by the piezoelectric actuator of the reference path. Phase shifts $\Delta\varphi_{2,ROI1}$ and $\Delta\varphi_{2,ROI2}$ differ from each other: in ROI1 the phase shift is introduced only by the piezoelectric actuator; in ROI2 an additional phase shift results from the reference object. From the difference in phase shifts $\Delta\varphi_{ref}=\Delta\varphi_{2,ROI2}-\Delta\varphi_{2,ROI1}$, the well known thickness of the reference object (d=3.00 mm) and the refractive indexes of BK7 glass n_{BK7} and air n_{air}, the artificial wavelength λ_a is calculated:

$$\lambda_a = \frac{2\pi}{\Delta\varphi_{ref}} d\left(n_{BK7} - n_{air}\right). \tag{9}$$

The phase shifts between subsequent interferograms of both ROIs must be in the range of 0 to π; the Cai *et al.* method is restricted to this range.

Alternatively, it is possible to capture three additional phase-shifted holograms with the phase object in the reference path and perform reconstruction with the Cai *et al.* three-step algorithm separately. Then the difference modulo 2π between the reconstructed phase maps in the hologram plane without [see Figs. 3 (a) and (c)] and with [see Figs. 3 (b) and (d)] reference objects, respectively, are calculated for both wavelengths. Figures 3(e) and (f) represent the phase shifts modulo 2π generated by the glass plate at both single wavelengths λ_1 and λ_2, respectively. Again these phase maps are subtracted modulo 2π from each other:

$$\Delta\varphi_{ref} = \left(\varphi_{\lambda 1} - \phi_{\lambda 1}\right) - \left(\varphi_{\lambda 2} - \phi_{\lambda 2}\right). \tag{10}$$

The result is shown in Fig. 3(g) and represents the phase map within the hologram plane at the generated artificial wavelength. Insertion of averaged phase difference $\Delta\varphi_{ref}$ between ROI1 and ROI2 in Eq. (9) allows for the calculation of the artificial wavelength.

D. Filtering

Because of the expansion of the complex hologram with zeros by a factor of 4 in each direction to perform propagation with the convolution method, the reconstructed complex object wave (amplitude and phase map) contains redundant information. With respect to the Abbe diffraction limit, the reconstructed complex object wave is oversampled. Hence it is useful to resize the image – real and imaginary parts separately – and to use the information of the redundant pixels to eliminate statistical noise. Here we simply calculated the mean value of the 4 by 4 pixel regions. Because filtering takes place below the diffraction limit, no physical information is lost.

4. Results

Measurement results of a set of generated artificial wavelengths between 5 mm and 35 mm are shown in Table. 1. For generation of the artificial wavelengths, the laser diode was tuned to approximately 250 pm to determine appropriate stable spectral modes. Respective single wavelengths λ_1 and λ_2 and the number of oscillating modes are monitored by a wavemeter. Speckle interferograms – three without and one with a reference object – were captured at each of the wavelengths, which ensured that images were recorded in single-mode operation of the diode laser. The generated artificial wavelength is calculated by Eq. (7) and compared with the artificial wavelength that was determined by the reference object method described by Eq. (9).

λ_1 [nm]	λ_2 [nm]	$\Delta\lambda$ [pm]	λ_a [mm] Wavemeter	λ_a [mm] Reference	Relative Error [%]
781.462	781.480	18	33.93	35.95	5.95
781.462	781.482	20	30.53	27.84	8.82
781.531	781.555	24	25.45	25.15	1.17
781.555	781.591	36	16.97	16.99	0.13
781.531	781.591	60	10.18	10.14	0.39
781.462	781.531	69	8.85	9.87	11.52
781.531	781.607	76	8.04	7.81	2.87
781.367	781.444	77	7.93	7.15	9.88
781.444	781.533	89	6.86	6.79	0.99
781.367	781.462	95	6.43	6.22	3.30
781.367	781.462	95	6.43	6.22	3.30
781.531	781.644	113	5.41	5.81	7.42

Table 1: Comparison of Measured Artificial Wavelengths with a Wavemeter and the Reference Object Method.

The relative error of the artificial wavelength between our reference object method and the wavelength measured with the wavemeter is listed in the rightmost column of Table 1. The measurement error (±0.5 pm) of the wavemeter corresponds to a relative error of the artificial wavelength below 1%. Comparison between wavemeter and reference object measurement of the artificial wavelength shows that our method works in principle, but it is obvious that we have some outliers with relative errors grater than 5%. In these cases we exceeded the range of validity (0 to π) of the global phase shift between speckle interferograms without and with reference objects in ROI1 or ROI2 in the Cai *et al.* algorithm [1]. This error can be avoided by using our described alternative method with the disadvantage of two additional interferogram recordings. In this case the relative error of the artificial wavelength measurement is in comparison with a wavemeter measurement always below 2%.
The test object in our measurement was a metallic shim with two cutouts of different heights (h_1=2.50 mm ± 0.01 mm, h_2=0.40 mm ± 0.01 mm). The tactile measurements of the step heights were taken with a digital micrometer caliper as the reference. An unambiguous measurement range of $\lambda_a/2$=5.07 mm (result of reference object measurement) was generated by two single wavelengths with 60 pm difference (λ_1=781.531 nm, λ_2=781.591 nm). The results of the reconstructed wave in the object

plane are shown in Fig. 4. In the amplitude images [Figs. 4(a) and 4(c)] the shim can be seen clearly. The corresponding phase images [Figs. 4(b) and (d)] display the random phase distribution of a speckle field that is due to the fact that the metallic surface is optically rough. By subtraction of these two images and applying Eq. (6), a difference phase map as shown in Fig. 5(b) can be calculated. To reduce the phase map to significant regions the areas around and in the middle of the metallic shim were masked out manually. Figure 5(c) displays a pseudo-3D plot of the measured height profile. Figure 5(a) again shows the reconstructed amplitude within the object plane at single wavelength λ_1. Unlike in Fig. 4(a), the gray values in Fig. 5(a) were scaled logarithmically to enhance image contrast.

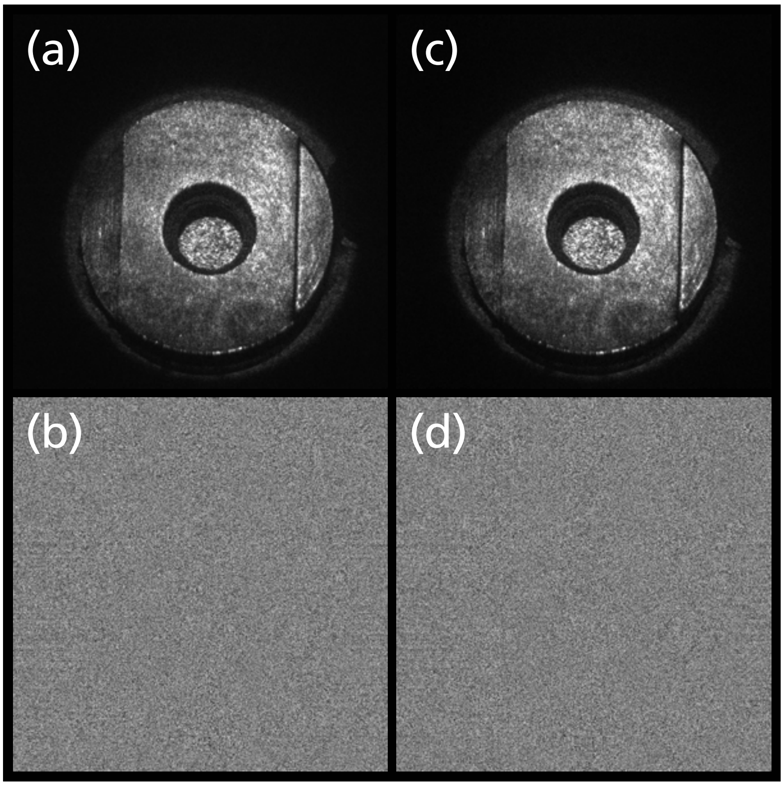

Fig. 4: Single wavelength reconstructions of amplitude and phase at (a), (b) λ=781.591 nm and (c), (d) λ=781.531 nm.

To approximate measurement accuracy the height profile extracted from the phase map of Fig. 5(b) along the marked cross section is plotted in Fig. 6. The maximum absolute deviation of the averaged phase value to the tactile measurement is less than 40 µm, whereas the statistical error (standard deviation) amounts 3σ=50 µm. In summary, we have an absolute error below 100 µm when using an artificial wavelength of 10 mm. The measurement time per wavelength is less than 1 s and is restricted by the frame rate of the image recording device and time for shifting the phase object partially into the reference path of the interferometer. The tuning time of the diode laser depends on the difference between the single wavelength and is in the 500 ms region. Numerical reconstruction is completely performed on a Graphic Processor Unit (N295GTX-1792MB) and takes less than 150 ms per wavelength using 4096 x 4096 sampling points in Eq. (4).

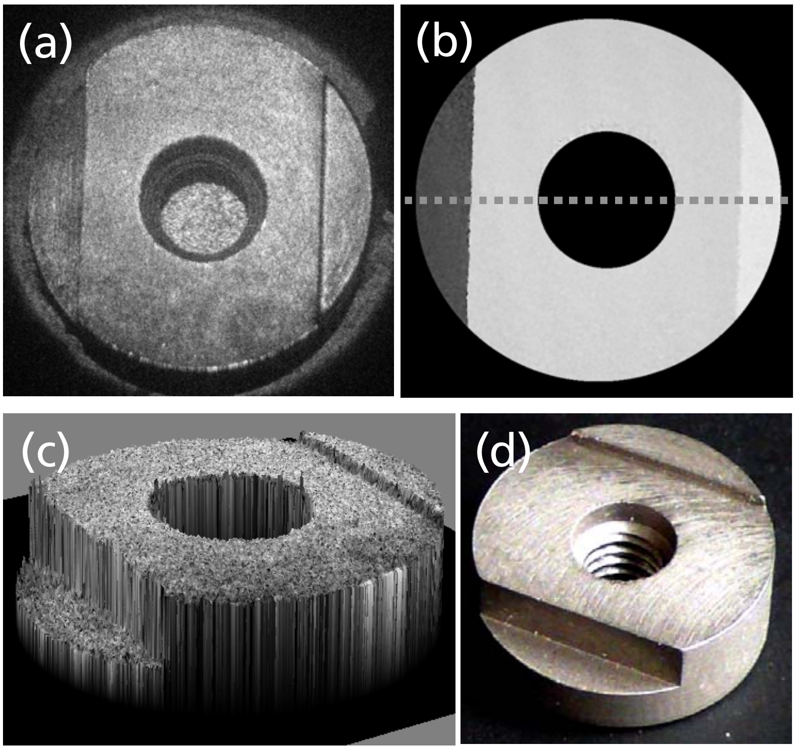

Fig. 5: (a) Reconstructed amplitude of the test object (gray values scaled logarithmically); (b) corresponding phase map of a generated artificial wavelength of 10.14 mm with cross section; (c) pseudo-3D representation of the phase map with the amplitude as a texture; (d) digital photograph of the test object.

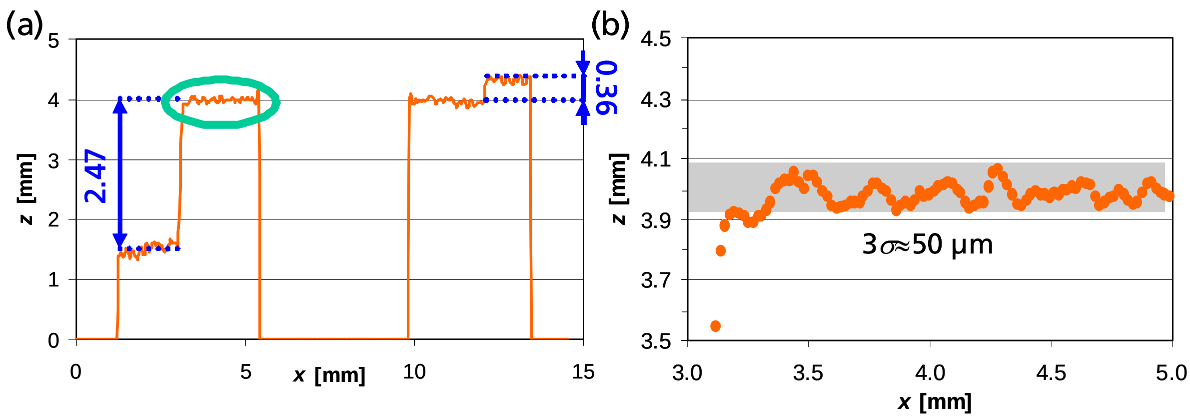

Fig. 6: (a) Height z versus lateral position x along the cross section marked in Fig. 5(b); (b) enlarged section of (a) with the 3σ range highlighted.

5. Conclusion

We have shown that the application of temporal phase shifting with unknown phase shifts is useful to suppress disturbances introduced by a twin image and zero-order diffraction in lensless digital holography. As a result, an uncontrolled piezostage can be used to achieve phase shifts by moving a mirror within the reference path of an interferometer. We have also shown that the algorithm used to calculate the phase shifts of adjacent speckle interferograms can also be used to determine the phase shift induced by a phase object moved partly into the reference path of an interferometer. The phase shift of the reference object can be used to calibrate the setup by determination of the generated artificial wavelength. We pointed out that the restriction to a range of validity between 0 and π between adjacent phase shifts in the Cai *et al.* algorithm must be considered. Nevertheless this problem can be overcome by applying a reference object with areas of different thicknesses, in which case we expect a relative accuracy of approximately 1% artificial wavelength measurements.
Finally, the presented results demonstrate that shape measurements with the autocalibrated setup of optically rough surfaces with an absolute accuracy better than one hundredth of the generated artificial wavelength are possible.
In conclusion, our results show the applicability of the described autocalibration methods for the unknown phase steps and the generated artificial wavelengths. Hence expensive devices such as closed-loop piezocontroller and a wavemeter become dispensable, which makes the setup more applicable to industrial environments. Furthermore, acceleration of numerical reconstruction by implementation of all calculations on a graphic processor unit enables the potential of the technique to be used in production lines with high throughput. Hologram recording can be accelerated by the use of appropriate camera hardware that is readily available commercially.

References

1. L. Z. Cai, Q. Liu, X. L. Yang: "Generalized phase-shifting interferometry with arbitrary unknown phase steps for diffraction objects", Opt. Lett. **29,** 183-185 (2004).
2. Y. I. Ostrovsky, M. M. Butusov, and G. V. Ostrovskaya, *Interferometry by Holography*, Springer Series in Optical Sciences (Springer, 1980).
3. Y. I. Ostrovsky, V. V. Shchepinov, and V. V. Yakovlev, *Holographic Interferometry in Experimental Mechanics*, Springer Series in Optical Sciences (Springer, 1991).
4. U. Schnars and W. Jüptner, "Direct recording of holograms by a CCD target and numerical reconstruction", Appl. Opt. **33,** 179-181 (1994).
5. M.-A. Beeck and W. Hentschel, "Laser metrology – a diagnostic tool in automotive development processes", Opt. Lasers Eng. **34**, 101–120 (2000).
6. V. P. Shchepinov and V. S. Pisarev, *Strain and Stress Analysis by Holographic and Speckle Interferometry* (Wiley, 1996).
7. T. Kreis, *Holographic Interferometry: Principles and Methods* (Akademie Publishing, 1996).
8. D. Carl, B. Kemper, G. Wernicke, and G. von Bally, "Parameter-optimized digital holographic microscope for high resolution living-cell analysis", Appl. Opt. **43**, 6536–6544 (2004).
9. Michael Liebling, T. Blu, and M. Unser, "Complex-wave retrieval from a single off-axis hologram", J. Opt. Soc. Am. A **21**, 367-377 (2004).
10. C. Mann, L. Yu, C.-M. Lo, and M. Kim, "High-resolution quantitative phase-contrast microscopy by digital holography," Opt. Express **13**, 8693–8698 (2005).
11. P. Marquet, B. Rappaz, P. J. Magistretti, E. Cuche, Y. Emery, T. Colomb, and C. Depeursinge, "Digital holographic microscopy: a noninvasive contrast imaging technique allowing quantitative visualization of living cells with subwavelength axial accuracy", Opt. Lett. **30**, 468–470 (2005).
12. B. Kemper, D. Carl, A. Höink, G. von Bally, I. Bredebusch, and J. Schnekenburger, "Modular digital holographic microscopy system for marker-free quantitative phase contrast imaging of living cells", Proc. SPIE **6191**, 61910T (2006).

13. E. Cuche, P. Marquet, and C. Depeursinge, "Simultaneous amplitude-contrast and quantitative phase-contrast microscopy by numerical reconstruction of Fresnel off-axis holograms", Appl. Opt. **38**, 6994–7001 (1999).
14. M.Kemmler, M. Fratz, D. M. Giel, N. Saum, A. Brandenburg, C. Hoffmann, "Noninvasive time-dependent cytometry monitoring by digital holography", J. Biomed. Opt. **12**, 064002 (2007).
15. B. Rappaz, P. Marquet, E. Cuche, Y. Emery, C. Depeursinge, and P. Magistretti, "Measurement of the integral refractive index and dynamic cell morphotometry of living cells with digital holographic microscopy", Opt. Express **13**, 9361–9373 (2005).
16. B. Kemper, D. Carl, J. Schnekenburger, I. Bredebusch, M. Schäfer, W. Domschke, and G. von Bally, "Investigation of living pancreas tumor cells by digital holographic microscopy", J. Biomed. Opt. **11**, 034005 (2006).
17. B. Rappaz, P. Marquet, E. Cuche, Y. Emery, C. Depeursinge, and P. J. Magistretti, "Measurement of the integral refractive index and dynamic cell morphometry of living cells with digital holographic microscopy", Opt. Express, **13**, 9361-9373 (2005).
18. D. C. Ghighlia and M. D. Pritt, "Two-Dimensional Phase Unwrapping: Theory, Algorithms, and Software", (Wiley-Interscience, 1998).
19. M. Takeda and H. Yamamoto, "Fourier-transform speckle profilometry: three-dimensional shape measurements of diffuse objects with large height steps and/or spatially isolated surfaces", Appl. Opt. **33**, 7829-7837 (1994).
20. S. Kuwamura and I. Yamaguchi, "Wavelength scanning profilomery for real-time surface shape measurement", Appl. Opt. **36**, 4473-4482 (1997).
21. C. Furlong and R. J. Pryputniewicz, "Absolute shape measurements using high-resolution optoelectronic holography methods", Opt. Eng. **39**, 216-223 (2000).
22. C. Wagner, W. Osten, and S. Seebacher, "Automatic processing of direct shape measurement by digital wavefront reconstruction and multiwavelength contouring", Opt. Eng. **39**, 79-85 (2000).
23. E. A. Barbosa, A. A. V. Filho, M. R. R. Gesualdi, B. G. Curcio, M. Muramatsu, and D. Soga, "Single-exposure, photorefractive holographic surface contouring with multiwavelength diode lasers", J. Opt. Soc. Am. A **22**, 2872-2879 (2005).
24. D. Parshall and M. Kim, "Digital holographic microscopy with dual-wavelength phase unwrapping", Appl. Opt. **45**, 451-459 (2006).
25. A. Wada, M. Kato, and Y. Ishii, "Large step-height measurements using multiple-wavelength holographic interferometry with tunable laser diodes", J. Opt. Soc. Am. A **25**, 3013-3020 (2008).
26. D. Carl, M. Fratz, D. Strohmeier, D. M. Giel, and H. Höfler, "Digital holography with arbitrary temporal phase-shifts and multiple wavelengths for shape measurement of rough surfaces", in *Digital Holography and Three-Dimensional Imaging, OSA Technical Digest (CD)* (Optical Society of America, 2008), paper DMC7.
27. L. Ricci, M. Weidemüller, T. Esslinger, A. Hemmerich, C. Zimmermann, V. Vuletic, W. König, and T.W. Hänsch, "A compact grating-stabilized diode laser system for atomic physics", Opt. Commun. **117**, 541-549 (1995).
28. R. Jones, "The design and application of a speckle pattern interferometer for total plane strain field measurement", Opt. Laser Technol. **8**, 215-219 (1976).
29. T. M. Kreis, M Adams, and W. P. O. Jueptner, "Methods of digital holography: a comparison", Proc. SPIE **3098**, 224-245 (1997).
30. D. Mas, J. Garcia, C. Ferreira, L. M. Bernardo, F. Marinho, "Fast algorithms for free-space diffraction patterns calculation", Opt. Commun. **164**, 233–245 (1999).
31. T. Shimobaba, Y. Sato, J. Miura, M. Takenouchi, and T. Ito, "Real-time digital holographic microscopy using the graphic processing unit", Opt. Express **16**, 11776-11781 (2008).